デジタル倒立顕微鏡に搭載したHCA用アプリケーションの技術と実施例の紹介

林　耕磨，門井宏平，柴田美智太郎，大井宏美，星野哲朗

Introduction of HCA Application Technology and Examples Installed on Digital Inverted Microscopes

Kohma HAYASHI, Kohei KADOI, Michitaro SHIBATA, Hiromi OI and Tetsuro HOSHINO

創薬分野において，High Content Analysis（HCA）と呼ばれる顕微鏡観察により薬剤の効果を評価する技術は，重要性を増してきている．一方で，HCA を実施するためには，細胞培養，画像取得，解析等の高度な専門知識が必要となる．ニコンは，誰でも簡単に HCA を実施できるようにするため，デジタル倒立顕微鏡 ECLIPSE Ji と，本顕微鏡専用ソフトウェア，NIS-Elements SE（Smart Experiment）を開発した．本稿では，Smart Experiment に搭載された技術の紹介と，実際の撮像例に関して紹介する．1 章にて背景を説明し，2 章では Smart Experiment を利用したときの画像取得から解析結果表示までのシステムワークフローを紹介する．3 章では，Smart Experiment のシステムワークフローを実現するために開発した，CellFinder.ai によるオートフォーカス技術と NIS.ai による細胞セグメンテーション技術を紹介する．4 章では，Size and Morphological analysis と Cytotoxicity の実施例を紹介することで，Smart Experiment にてどのような実験結果を出力できるか示す．最後に 5 章では，本技術を振り返って，今後の展望について説明したい．

In drug discovery, High Content Analysis (HCA), a microscope-based drug efficacy evaluation screening approach, is becoming increasingly important with imaging technology development. However, performing HCA requires advanced expertise in several fields (e.g., cell culture, image acquisition, analysis, etc.). Nikon developed a digital inverted microscope, ECLIPSE Ji, and corresponding software, NIS-Elements SE (Smart Experiment), for easy HCA execution using this microscope. In this study, we introduce the technology installed in Smart Experiment, along with actual imaging examples. Chapters 1 and 2 introduce the background and workflow from image acquisition to analysis result display when using Smart Experiment, respectively. Chapter 3 discusses the autofocus and cell segmentation technologies by CellFinder.ai and NIS.ai, respectively (both developed to realize Smart Experiment). Chapter 4 presents size and morphological analyses as well as cytotoxicity examples as actual assays. Finally, Chapter 5 provides a future outlook.

Key words 顕微鏡，深層学習，自動化，ライフサイエンス，創薬
microscope, deep learning, automation, life science, drug discovery

1 Introduction

Image analysis techniques for evaluating the effects of drugs through microscopic observation are known as high content analysis (HCA). Conducting HCA, which requires various advanced expertise, is becoming increasingly important in the field of drug discovery alongside developments in imaging technology [1]. Expertise requirements include knowledge of preparing cell samples and constructing experimental systems for drug evaluation, knowledge of acquiring quantitative microscopic images, knowledge of image processing to extract features from captured images, and knowledge of statistical analysis to present drug effects from the extracted features. Given the need for such complex knowledge, HCA has the problem of having high barriers to entry for those who are conducting it for the first time. Nikon has sought to solve this problem by developing a digital inverted microscope called ECLIPSE Ji and software dedicated to this microscope called NIS-Elements SE (Smart Experiment) as a system for automating the complex workflow involved in conducting HCA. In this paper, we introduce the technologies installed in Smart Experiment and demonstrate an actual example of conducting HCA.

2 Smart Experiment System Workflow

In this section, we briefly introduce the Smart Experiment system workflow. In NIS-Elements SE, the imaging and analysis proceed according to the system workflow depicted in Fig. 1 so that the user can conduct the assay without having to configure various settings. Each step is explained below.

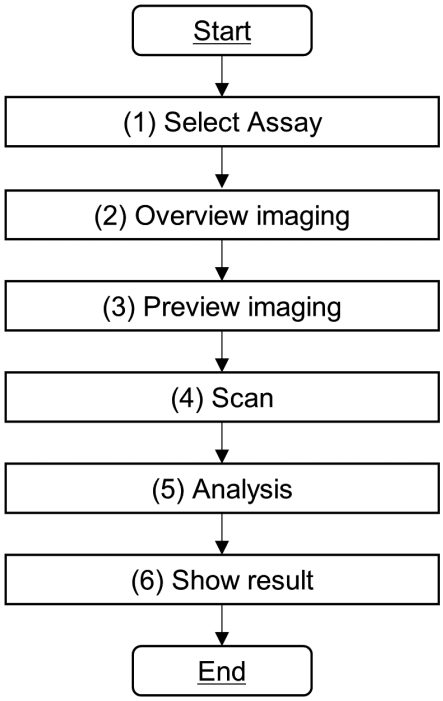

Fig. 1 Smart Experiment workflow overview

(1) Select Assay

After initial preparation of the sample, it is mounted on the stage of Ji and the corresponding assay is selected from the SE mode of NIS-Elements.

(2) Overview Imaging

The system determines how many wells the sample placed by the user is in, and the XY tilt of the plate is corrected.

An image is acquired at the center of each well to detect the presence of cells. Next, the cell density and the bias within the field of view of this image are analyzed to detect the optimal field of view for high-magnification observation.

(3) Preview Imaging

Subsequently, automatic illumination condition adjustment is conducted using AI (Autosignal.ai), either for the wells selected by the user or for all the wells within the imaging range. This result is used as a basis to calculate the illumination conditions (LED power, exposure time) that will not saturate the brightness of the brightest well among the scanned wells. Autofocus is also conducted in the bright field on the first well to be scanned initially; subsequently, autofocus is conducted for each fluorescent channel of the images. These autofocus results are used to calculate the offset value between the focal position in the bright field caused by axial chromatic aberration and the focal position for each fluorescent channel. AI-based bright field autofocus (CellFinder.ai) is used to calculate the bright field focus.

(4) Scan

The image to be used for analysis is acquired using the XY position determined in *Overview Imaging*, the illumination conditions determined in *Preview Imaging*, and the offset value of each fluorescent channel from the bright field.

(5) Analysis

The analysis recipe defined for each assay is executed for the image captured during *Scan* step.

(6) Show Result

Finally, the analysis results are displayed on the result display screen.

3 AI Technologies used in Smart Experiment

In this section, we introduce the AI technologies installed in Smart Experiment.

3.1. Autofocus by CellFinder.ai

3.1.1. Principle Overview

Conventional autofocus methods used in microscopes follow a method in which the focal plane is determined from the brightness information of each image while acquiring images in the Z direction. The conventional method requires the focal plane to be within the Z operation range, so an appropriate Z range must be set in advance. When this range is narrow, the Z operation will not reach the focal plane, leading to autofocus failure. Conversely, when the Z range is set too wide, the autofocus process lasts unnecessarily over a long time.

We avoided the above issues by developing a new autofocus method for Smart Experiment. As shown in Fig. 2, this method uses a procedure for estimating the distance to the focal plane from two images with different Z positions. A deep neural network (DNN) is used for estimating the focal plane.

3.1.2. Training Method

Z-stack images were acquired for each objective lens, and the distance to the focal plane was labeled for two images with different Z positions for learning. The cell types in Table 1 were used for training. The focal plane in the bright field observation was defined as the Z position where the contrast was at a local minimum.

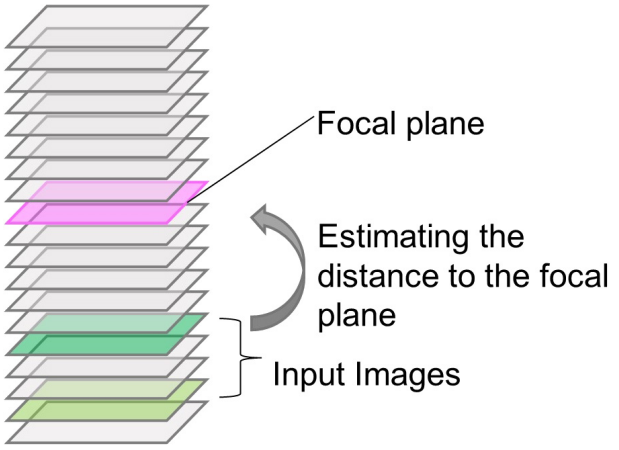

Fig. 2 Principle of CellFinder.ai

Table 1 The cell types used for CellFinder.ai

Cell Type	Origin
HeLa	RIKEN BRC, RCB0007
HepG2	JRCB cell bank, JCRB1054
HT-29	ATCC, HTB-38
COS-7	RIKEN BRC, RCB0539
CHO-K1	JRCB cell bank, JCRB9018
A-431	NIHS, JCRB 0004
Neuro2a	ATCC, CCL-131
iPSC derived Neurons	Elixirgen Scientific, EX-SeV-CW50065
BS-C-1	NIHS, JCRB9126
J774.1	NIHS, JCRB0018

3.1.3. Performance

The error from the focal plane was evaluated using 3 × SD (standard deviation). The verification was conducted in the range of ± 250 μm from the focal plane. Table 2 shows the evaluation results.

Table 2 The evaluation results of the CellFinder.ai

Objective lens	Error range from the focal plane (± 3 × SD)
Plan Apo λD 4x	< ± 10 μm
Plan Apo λD 10x	< ± 8 μm
Plan Apo λD 20x	< ± 5 μm

3.2. Cell Segmentation using NIS.ai

3.2.1. Principle Overview

The first step in analyzing the images captured by the microscope requires the segmentation of the measurement targets, e.g. the cell nuclei and cell regions. The images are generally binarized by setting a brightness threshold, and post-processing such as morphological transformation is added to segment only the measurement target object. However, this method requires parameters such as the threshold to be fine-tuned depending on the imaging conditions and subtle differences in sample preparation conditions (e.g., staining time, concentration of staining reagent, time since reagent was opened). Complex image processing processes must also be considered to extract the cell nuclei and cell regions from the bright field and phase contrast images.

Meanwhile, segmentation methods using DNNs, such as Pixel2Pixel and U-net, have emerged in recent years and are beginning to be used for cell samples [2]. Our company's NIS-Elements also includes the aforementioned DNN-based segmentation technology in the form of Segmentation.ai and ObjectSegment.ai in NIS.ai. Advantages of this method are that it does not require parameter adjustments by training in advance the differences in samples that occur due to differences in experimental conditions. Moreover, less time is needed for analysis than conventional methods due to the GPU-based calculations. Because the detailed principles and application examples of this method have already been published in Nikon Research Report Vol. 3, they have been excluded from this paper.

3.2.2. Training Method

NIS-Elements SE is equipped with four types of learning models: two training models that segment cell nuclei and cell regions from fluorescent images, and two training models that segment cell nuclei and cell regions from bright field images. A binary image segmented from a fluorescent image using a conventional method as a training image was used to create a segmentation model from a fluorescent image. Initially, a fluorescently stained sample was prepared, bright field and fluorescent images were captured, and the fluorescent image was segmented using a conventional method for creating a training image to create a segmentation model from a bright field image. Similarly, an image in which the cell nucleus was stained with Hoechst33342 (Nacalai Tesque, Kyoto, Japan, 19172-51) was utilized for cell nucleus segmentation, and an image in which the cell region was stained with CellMask™ Deep Red (Thermo Fisher Scientific, Massachusetts, US, C10046) was used for cell region segmentation. The SegmentObject.ai function was used for cell nucleus training, and mainly the Segment.ai function for cell region training. Table 3 lists the cell types used in learning.

Table 3 The list of the cell types used for AI trainning

Cell type	Origin
HeLa	RIKEN BRC, RCB0007
HepG2	JRCB cell bank, JCRB1054
COS-7	RIKEN BRC, RCB0539
CHO-K1	JRCB cell bank, JCRB9018
A-431	NIHS, JCRB 0004
J774.1	NIHS, JCRB0018
Neuro2a	ATCC, CCL-131

3.2.3. Evaluation Method

The segmentation model created using NIS.ai was subjected to a sensory evaluation and quantitative evaluation by confirming the appearance of the detected region when applied to the image of the trained cell type. Data obtained separately from the training data were used for the evaluation. For the model to detect cell nuclei, the ratio of the number of nuclei detected by the segmentation model to the number of cell nuclei detected from the fluorescent image of Hoechst33342 (Nacalai Tesque) was calculated, and it was confirmed that the ratio was 90–110% (Fig. 3(B)). For the segmentation model to detect cell regions, the ratio of the area of the cell region detected by the segmentation model to the area of the cell region detected from the fluorescent image of CellMask™ Deep Red (Thermo Fisher Scientific) was also confirmed to be in the range of 90–110% (Fig. 3(C)). In addition to conducting accuracy evaluations of the segmentation model, a comprehensive evaluation was carried out to confirm that the difference between the positive and negative controls prepared under the conditions recommended by Nikon for the intended use of the assay was sufficiently detectable. The Z'-factor, which is an index of system stability, was used as an evaluation criterion [1].

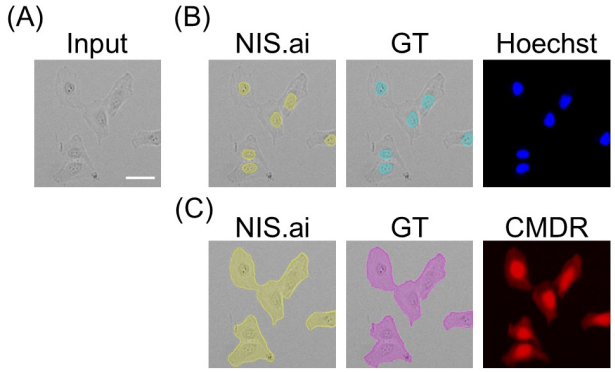

Fig. 3 Region detection by NIS.ai segmentation model
(A) Bright field image input to NIS.ai. Scale bar is 50 μm. (B) From left, nuclear region inference result by NIS.ai (yellow region), ground truth of the nuclear region detected from Hoechst33342 fluorescent image (light blue region), and Hoechst33342 fluorescent image (blue). (C) From left, the cell region inference result by NIS.ai (yellow region), ground truth of cell region detected by CellMask™ Deep Red fluorescent image (magenta region), and CellMask™ Deep Red fluorescent image (red).

4 Examples of Assays using Smart Experiment

In this section, we introduce examples of measurements made using Smart Experiment.

4.1. Cell Morphology Analysis using Size and Morphological Analysis

4.1.1. Assay Overview

Cells undergo various morphological changes during physiological phenomena. For example, cell enlargement is known to progress with cell aging caused by DNA damage, oxidative stress, and cancer gene activation [3]. Screening drugs that target cascades related to such cell morphological changes and evaluating toxicity to cells using cell morphology as an index are important. The purpose of this assay is to provide an application that can measure the morphological features such as the size, circumference, and circularity of cells and cell nuclei.

In this assay, images are acquired using a 10x objective lens for image analysis, and morphological features are measured by segmenting the cell nucleus region and cell region from the fluorescent images of the cell nucleus and cell region, respectively.

4.1.2. Evaluation Experiment Overview

In the evaluation experiment of this assay, the concentration dependency of cell size was verified using camptothecin (Sigma-Aldrich, Missouri, US), which is an inhibitor of DNA topoisomerase I. HeLa cells were seeded in a 96-well plate (AGC Technoglass, Shizuoka, Japan 5866-096) and cultured. Subsequently, culturing was conducted for 24 hours in a medium containing a dilution series of camptothecin (Sigma-Aldrich) (0–1000 nM, 10 concentration points). Finally, the cells were fixed with 4% PFA, and the cell nuclei were stained with Hoechst 33342 and the cell membranes with CellMask™ Deep Red (Thermo Fisher Scientific) [4].

The sample plate was mounted in the Ji, and a Size and Morphological Analysis assay was conducted. To calculate the Z'-factor, a 0 nM camptothecin (Sigma-Aldrich) range was set as a negative control, and a 333 nM camptothecin (Sigma Aldrich) range was set as a positive control. Six replicate wells were setup for each concentration, and the experiment was conducted thrice as biological replicates.

4.1.3. Evaluation Results

Figure 4 presents the evaluation results.

The representative image examples at each concentration point are shown in Fig. 4(A), the heat map of cell area shown in Fig. 4(B), and the concentration dependence curve shown in Fig. 4(D) confirmed that the cell area increases in a concentration-dependent manner. As shown in Fig. 4(C), the Z'-factor was > 0.5 (0.52), thereby confirming that the assay exhibited sufficient performance. Additionally, the EC50 in this experiment was 12.8 nM.

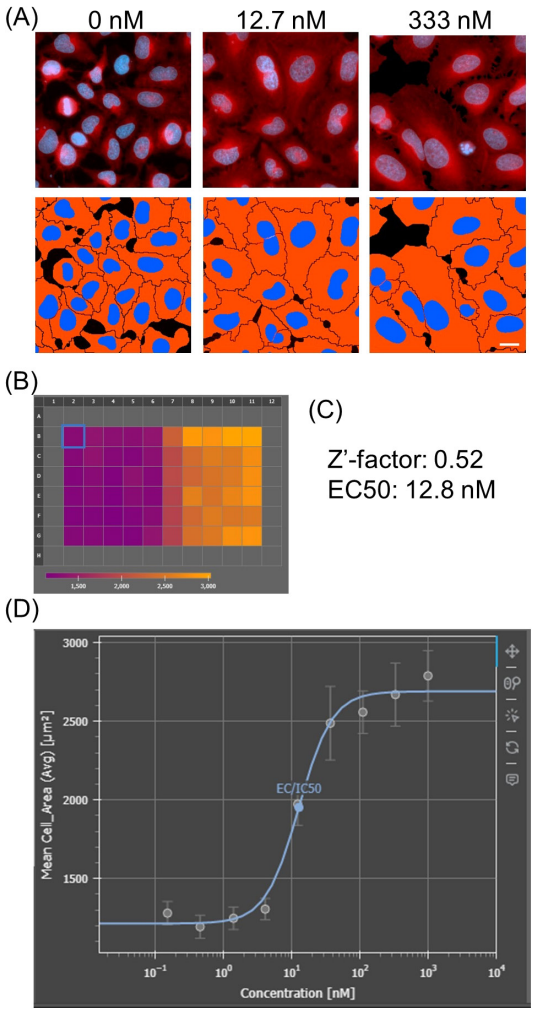

Fig. 4　Size and Morphological Analysis evaluation results
(A) Cell images at concentrations of 0, 12.7, and 333 nM from the left. The top row shows an image of brightness only (blue: Hoechst33342, red: CellMask™ Deep Red), and the bottom row shows the segmented mask (blue: cell nucleus region, red: cell region). The scale bar is 20 µm. (B) Cell area shown in a heat map. (C) Calculation results of Z'-factor and EC50 when cell area is used as index. (D) Concentration dependence curve with cell area on vertical axis and camptothecin concentration on horizontal axis. The error bars indicate standard deviation between replicates. The blue line indicates the fitting of a plot to a sigmoid curve.

4.2. Drug Toxicity Evaluation Results using Cytotoxicity

4.2.1. Assay Overview

Evaluating cytotoxicity is important for evaluating drugs, culture conditions, environment, and other stresses on cells. The purpose of this assay is to measure the percentage of stained dead cells.

In this assay, images are acquired using a 10x objective lens for image analysis, and the total number of cells and the number of dead cells are determined from the fluorescent images of cell nuclei and dead cells, from which the ratio of the live to dead cells is calculated.

4.2.2. Evaluation Experiment Overview

The evaluation experiment of this assay involved the use of a protein kinase inhibitor such as staurosporine (Sigma Aldrich, Missouri, US) to induce cell death and the verification of the concentration dependence of the number of dead cells [5]. HeLa cells were seeded in a 96-well plate (AGC Technoglass) and cultured. Subsequently, culturing was conducted for 24 hours in a medium containing a dilution series of staurosporine (Sigma-Aldrich) (0–1000 nM, 10 steps).

Finally, the cell nuclei were then stained with Hoechst33342 (Nacalai Tesque), whereas the dead cells

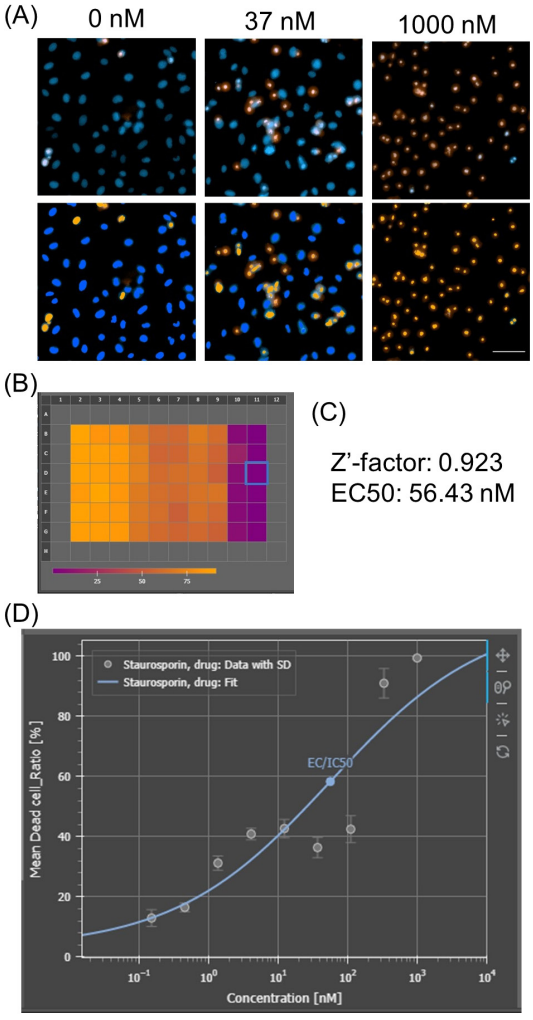

Fig. 5　Cytotoxicity evaluation results
(A) Cell images at concentrations of 0, 37, and 1000 nM from the left. The top row shows an image of brightness only (blue: Hoechst33342, red: EthD-1), and the bottom row shows the segmented mask (blue: live cells, orange: dead cells). The scalebar is 100 µm. (B) Cell death rate shown in a heat map. (C) Calculation results of Z'-factor and EC50 when cell area is used as index. (D) Dose response curve with cell area on the vertical axis and staurosporine (Sigma Aldrich) concentration on the horizontal axis. The error bars indicate standard deviation between replicates. The blue line indicates the fitting of a plot to a sigmoid curve.

were stained with ethidium homodimer-1 (EthD-1) (Thermo Fisher Scientific, Massachusetts, US, L3224).

The sample plate was mounted in the Ji, and a Cytotoxicity assay was conducted. To calculate the Z'-factor, a 0 nM staurosporine (Sigma Aldrich) range was set as a negative control, and a 1000 nM staurosporine (Sigma Aldrich) range was set as a positive control. Six replicate wells were setup for each concentration, and the experiment was conducted thrice as biological replicates.

4.2.3. Evaluation Results

Figure 5 shows the evaluation results.

The representative image examples at each concentration point shown in Fig. 5(A), the heat map of the Dead cell ratio shown in Fig. 5(B), and the dose responce curve shown in Fig. 5(D) confirmed that the cell death rate increased in a concentration-dependent manner. As shown in Fig. 5(C), the Z'-factor was > 0.5 (0.923), thereby confirming that the assay exhibited sufficient performance. Additionally, the EC50 in this experiment was 56.43 nM.

5 Conclusion

NIS-Elements SE makes it easy to conduct assays using the newly installed AI functions. In this paper, we introduced the kinds of measurements that are possible using the AI technologies installed in NIS-Elements SE as well as the two assays Size and Morphological Analysis and Cytotoxicity. There are 11 other assay types installed as of the time of writing this paper, and they can be used in many cell-evaluation experiments. We will continue to expand the functions and types of assays with the aim of contributing to the efficiency of the research, particularly in the field of drug discovery and the search for new drugs.

References

[1] W. Buchser, M. Collins, T. Garyantes, R. Guha, S. Haney, V. Lemmon, Z. Li, and O. J. Trask, "Assay Development Guidelines for Image-Based High Content Screening, High Content Analysis and High Content Imaging," *Assay Guidance Manual*, 2012.

[2] T. Falk, D. Mai, R. Bensch, Ö. Çiçek, A. Abdulkadir, Y. Marrakchi, A. Böhm, J. Deubner, Z. Jäckel, K. Seiwald, A. Dovzhenko, O. Tietz, C. D. Bosco, S. Walsh, D. Saltukoglu, T. L. Tay, M. Prinz, K. Palme, M. Simons, I. Diester, T. Brox, and O. Ronneberger, "U-Net: deep learning for cell counting, detection, and morphometry," *Nature Methods*, vol. 16, pp. 67–70, 2019.

[3] R. Katasho, T. Nagano, T. Iwasaki, and S. Kamada, "Nectin-4 regulates cellular senescence-associated enlargement of cell size," *Scientific Reports*, vol. 13, 21602, 2023.

[4] Y. Futamura, M. Kawatani, S. Kazami, K. Tanaka, M. Muroi, T. Shimizu, K. Tomita, N. Watanabe, and H. Osada, "Morphobase, an encyclopedic cell morphology database, and its use for drug target identification," *Chemistry & Biology*, vol. 19, no. 12, pp. 1620–1630, 2012.

[5] H. -J. Chae, J. -S. Kang, J. -O. Byun, K. -S. Han, D. -U. Kim, S. -M. Oh, H. -M. Kim, S. -W. Chae, H. -R. Kim, "Molecular mechanism of staurosporine-induced apoptosis in osteoblasts," *Pharmacologial Res.*, vol. 42, no. 4, pp. 373–381, 2000.

林　耕磨　Kohma HAYASHI
ヘルスケア事業部 技術統括部 システム開発部
System Development Department
Technology Solutions Sector
Healthcare Business Unit

門井宏平　Kohei KADOI
ヘルスケア事業部 技術統括部 システム開発部
System Development Department
Technology Solutions Sector
Healthcare Business Unit

柴田美智太郎　Michitaro SHIBATA
ヘルスケア事業部 技術統括部 システム開発部
System Development Department
Technology Solutions Sector
Healthcare Business Unit

大井宏美　Hiromi OI
ヘルスケア事業部 技術統括部 システム開発部
System Development Department
Technology Solutions Sector
Healthcare Business Unit

星野哲朗　Tetsuro HOSHINO
先進技術開発本部 数理技術研究所
Mathematical Sciences Research Laboratory
Advanced Technology Research & Development Division


林　耕磨
Kohma HAYASHI


門井宏平
Kohei KADOI


柴田美智太郎
Michitaro SHIBATA


大井宏美
Hiromi OI


星野哲朗
Tetsuro HOSHINO